

Supporting Information for

Natural gambogic acid-tuned self-assembly of nanodrug towards synergistic chemophototherapy against breast cancer

Baohang Lin^{#a}, Xun Peng^{#a}, Jianjun Cheng^{*b}, Jiacheng Wang^{*c}

^a Longgang Central Hospital of Shenzhen, Long Gang District, Shenzhen, PR China

^b Key Laboratory of Natural Medicine Innovation and Transformation, Henan University, Kaifeng, PR China

^c Medical College, Yangzhou University, Yangzhou, PR China

[#] These authors made equal contributions to this work.

***Corresponding author.**

Email: chengjj@henu.edu.cn (Jianjun Cheng); jcw@yzu.edu.cn (Jiacheng Wang).

Experimental Section.....	S2-S5
Supporting Figures.....	S5- S8
Table.....	S8
References.....	S9

Experimental section

1.1 Materials

Gambogic Acid (GA) was purchased from Nanjing Spring & Autumn Biological Engineering Co., Ltd (Nanjing, China). Pyropheophorbide-a (PPa), 4,6-diamino-2-phenyl-indole (DAPI), Tween 80, 3-(4,5-dimethylthiazol-2-yl)-2,5-diphenyl-tetrazolium bromide (MTT), Calcein-AM, and propidium iodide (PI) were purchased from the Aladdin Reagent Co. Ltd. (Shanghai, China). Dimethyl sulfoxide (DMSO) was purchased from Sinopharm Chemical Reagent Co., Ltd (Shang Hai, China). Fetal bovine serum (FBS), penicillin-streptomycin DMEM, and RPMI 1640 Medium were purchased from Sigma Gibco (Grand Island, NY, USA). All other chemicals, if not mentioned, were used as received.

1.2 Characterization

The mainly self-assembled reactions were performed on A KQ-100E ultrasonic cleaner. Scanning Electron Microscope (SEM) images were recorded on an aluminum foil plate using a JSM-7160F Plus electron microscope, and Transmission Electron Microscope (TEM) images were recorded on JEM-F200 (JEOL, Japan) operating at 200kV. UV-Vis absorption spectra were recorded at room temperature using a TU-1900 PERSEE spectrophotometer. Fluorescence emission spectra were performed with an F-2700 spectrometer. Particle size and zeta potential of samples were analyzed on a Zetasizer Nano ZS (Malvern Instruments Ltd., UK). And irradiation was performed using an MRFCL.660.T2.600.MM red laser (Mid-River, Xian, China). Cell imaging was acquired on a confocal laser scanning microscope (CLSM, Leica TCS SP8 STED), and MTT evaluation was performed with A BioTek Synergy H1 microplate reader.

1.3 PPa loading and encapsulation efficiency

The self-assembled nano-GA/PPa were first disassembled by dissolving in DMSO. Then, PPa and carrier GA in nano-GA/PPa were determined by HPLC (Agilent 1200 series liquid chromatography). For analysis, the reversed-phase TC-C18 column (4.6 mm i.d. × 250 mm, Agilent Technologies, USA) connected to an Agilent G1315B UV-Vis Detector was used at 30 °C. The PPa and GA concentrations were separately determined at 402 nm and 360 nm using 0.2% phosphoric acid water solution and acetonitrile as mobile phase at a flow rate of 1.0 mL/min, the corresponding volume

ratios were 20:80 and 10:90 for PPa and GA, respectively. The encapsulation efficiency (EE) and drug loading (DL) were calculated by the following equations:

$$DL (\%) = m_1 / (m_1 + m_2) \times 100\%$$

$$EE (\%) = m_1 / m_3 \times 100\%$$

Here, m_1 , m_2 , and m_3 represent the amount of PPa, GA in the precipitate, and input PPa, respectively.

1.4 Molecular dynamics simulation

The MD simulations were performed using the Materials Studio 8.0TM package.¹ Firstly, the energy-minimized structures of GA and PPa were simulated by density functional theory (DFT) (B3LYP, 6-31G (d, p)).² Secondly, eight GA molecules and two PPa molecules were randomly distributed in a water box sized $3.3 \times 3.3 \times 3.3 \text{ nm}^3$. The density was set to $1.0 \text{ g} \cdot \text{cm}^{-3}$. Thirdly, after initial energy minimization with 1000 steps of steepest descent minimization and subsequently annealing at NVE ensemble (298 K-500 K) for 20 ps, the system was performed for a total simulation of 1000 ps in an NVT ensemble using Forcite model block with Berendsen thermostat used. The simulation time step was 1 fs, and the particle mesh Ewald method was used to calculate electrostatic interactions. Meanwhile, the cut-off distance for nonbonded interaction was truncated at 12.5 Å. In all MD simulations, the COMPASS II force field was used.

1.5 Cell culture

Breast cancer cells 4T1 (mouse) and MCF-7 (human), liver hepatocellular cells (HepG2) were employed to evaluate the cell viability. MCF-7 and HepG2 cells were cultured in DMEM medium with 10% fetal bovine serum (FBS, Gibco) and 1% penicillin-streptomycin antibiotic (Life Technology, USA), while 4T1 cells were cultured in RMPI-1640 instead of DMEM medium. All cells were cultured under a 95% humidified atmosphere with 5% CO₂ at 37°C.

1.6 Cellular uptake of nano-GA/PPa

4T1 cells (10^5) were seeded in 35 mm confocal dishes and incubated for 24 h at 37 °C. Then, the culture medium was replaced with 1 mL of free PPa or nano-GA/PPa (equivalent PPa: 1 µg/mL) fresh medium, and further incubated for various periods (10 min, 1 h, and 3 h). After fixing and DAPI staining of the cells, then imaged under CLSM. In addition, the intracellular mean fluorescence was monitored by flow

cytometric analysis. Same as above cell treatments, the treated cells were successively harvested, centrifuged, washed, and re-suspended in 200 μ L of PBS, then 10^4 cells were analyzed using a Novocyte flow cytometer.

1.7 Cell apoptosis assay

Calcein AM/propidium iodide (PI) live/dead staining was performed to visualize the cytotoxicity of nano-GA/PPa. Briefly, 4T1 cells were seeded in 6-well plates incubated overnight. Then, the cells were treated with 1 mL of free PPa or nano-GA/PPa (PPa: 0.15 μ g/mL, GA: 0.75 μ g/mL) for 6 h. For the irradiation group, the cells were irradiated for 10 min immediately and incubated for another 1 h. After rinsing carefully, the cells were stained with Calcein AM (2 μ M)-PI (5 μ M) solutions for 20 min and observed under CLSM.

1.8 Animal models

Female Balb-c mice (18-22 g, 6-7 weeks old) were purchased from Huaxing Experimental Animal Center (Zhengzhou, China). 4T1 cells were suspended in RMPI-1640 medium, then subcutaneously injected into the right back of each mouse. All animal experiments were performed under protocols approved by the animal management and ethics committee of Henan University (Kaifeng, China).

1.9 Pharmacokinetics of nano-GA/PPa

Healthy Balb-c mice were (n=3) intravenously injected 200 μ L of free PPa or nano-GA/PPa (equivalent PPa: 3 mg/kg). At predetermined time intervals, 50 μ L of blood was withdrawn from posterior orbital venous plexus into heparinized tubes and added to 50 μ L of cold blood lysis buffer (strong RIPA, R0010, Solarbio). Subsequently, the mixture were vortexed and immediately lysed at 4 $^{\circ}$ C for 15 min. Then, the PPa in blood supernatant was collected by centrifugation at 12000 rpm, and the concentrations of PPa were further analyzed by HPLC as described above according to a standard curve of known amounts of PPa in blood. Drug and statistics software (DAS ver 2.0) was used for the analysis of pharmacokinetic parameters.

1.10 Biosafety evaluation

At the end of the treatment, the major organs (heart, liver, spleen, lung, and kidney) were harvested, fixed, and stained with H&E for histological analysis. Additionally, the mice's blood serum was collected carefully for serum biochemistry assay by

stewing at 4 °C for 2 h and following centrifugation at 3000 rpm. These markers were obtained including aspartate aminotransferase (AST), alanine aminotransferase (ALT), alkaline phosphatase (ALP), creatinine (CREA), uric acid (UA), blood urea nitrogen (BUN), albumin (ALB), and total bilirubin (TBIL).

1.11 Statistical analysis

All the data are expressed as the mean±standard deviation (SD) unless otherwise noted. Data were analyzed by t-tests with SPSS 22.0 software. The statistical differences were considered significant for * $P < 0.05$, ** $P < 0.01$, *** $P < 0.001$.

Supporting Figures

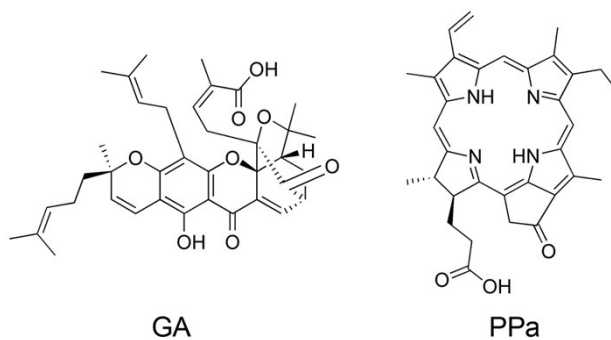


Figure S1. Molecular structures of GA and PPa, respectively.



Figure S2. The photographs of GA/PPa reaction water solution at different molar ratios of GA to PPa.

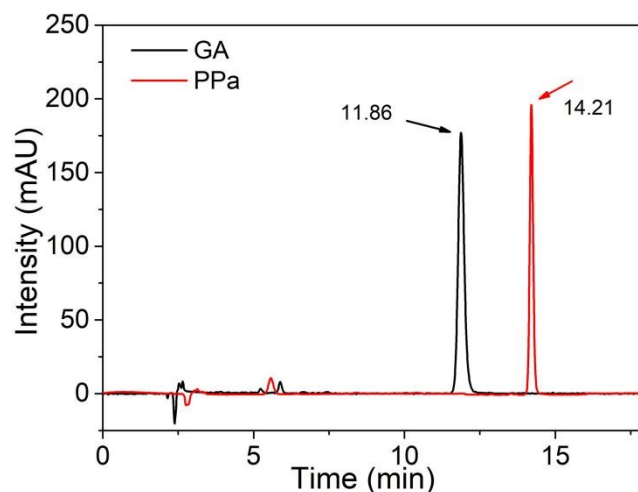


Figure S3. HPLC of GA of PPa at a mobile phase contained 0.2% phosphoric acid aqueous solution and acetonitrile (10:90 for GA and 20:80 for PPa, v/v) with a flow rate of 1.0 mL/min, while the detection wavelength was 360 nm and 402 nm, respectively.

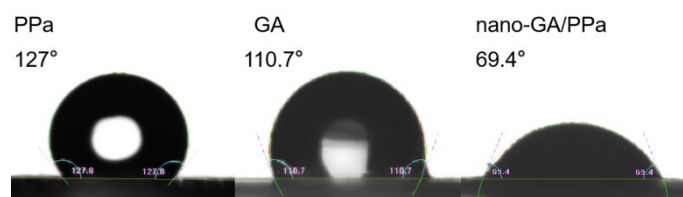


Figure S4. The contact angle of free GA, PPa, and nano-GA/PPa, respectively.

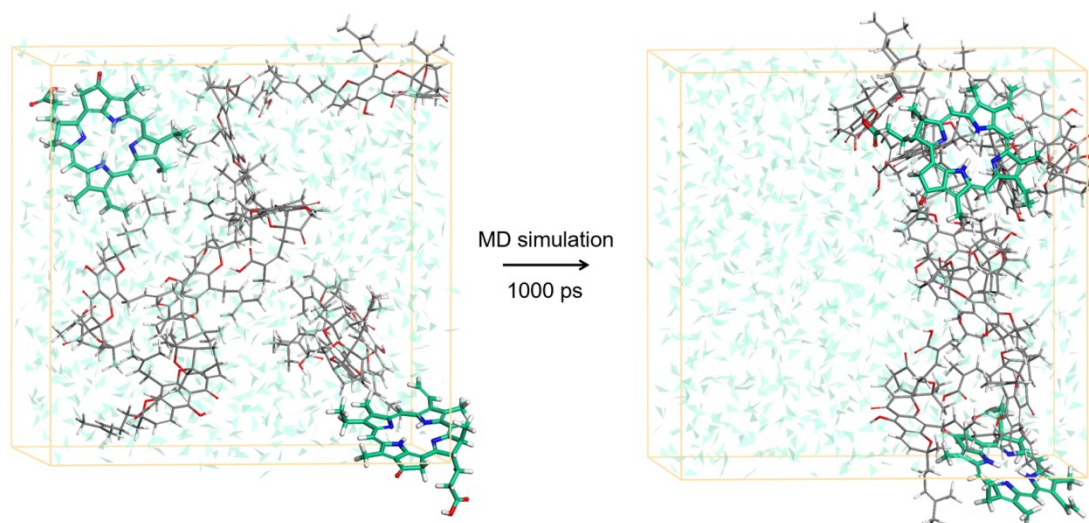


Figure S5. Structure of co-assembled nano-GA/PPa (GA: PPa =4:1) obtained by MD simulation for a total of 1000 ps. Water molecules are labeled with light green. The line and ball models were separately used for the GA and PPa molecules.

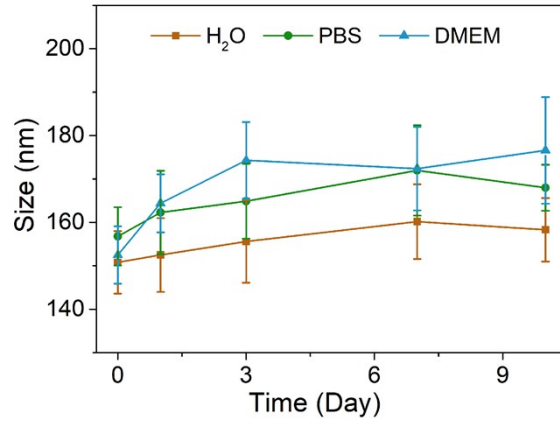


Figure S6. Size change of nano-GA/PPa over time in PBS, H₂O, and DMEM culture medium. The slight increase in average diameter may be due to nano-aggregation induced by the small size effect.

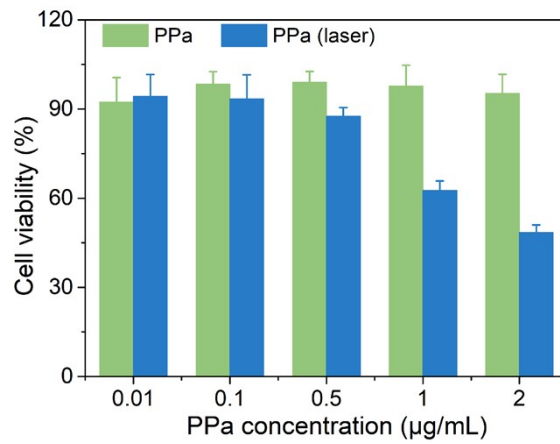


Figure S7. Cytotoxicity of PPa with or without laser against 4T1 cells after incubation for 24 h.

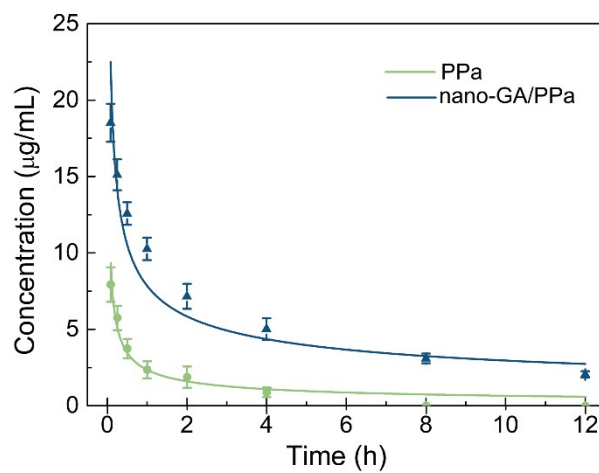


Figure S8. PPa concentration–time profiles in the blood after intravenous injections of nano-GA/PPa or free PPa.

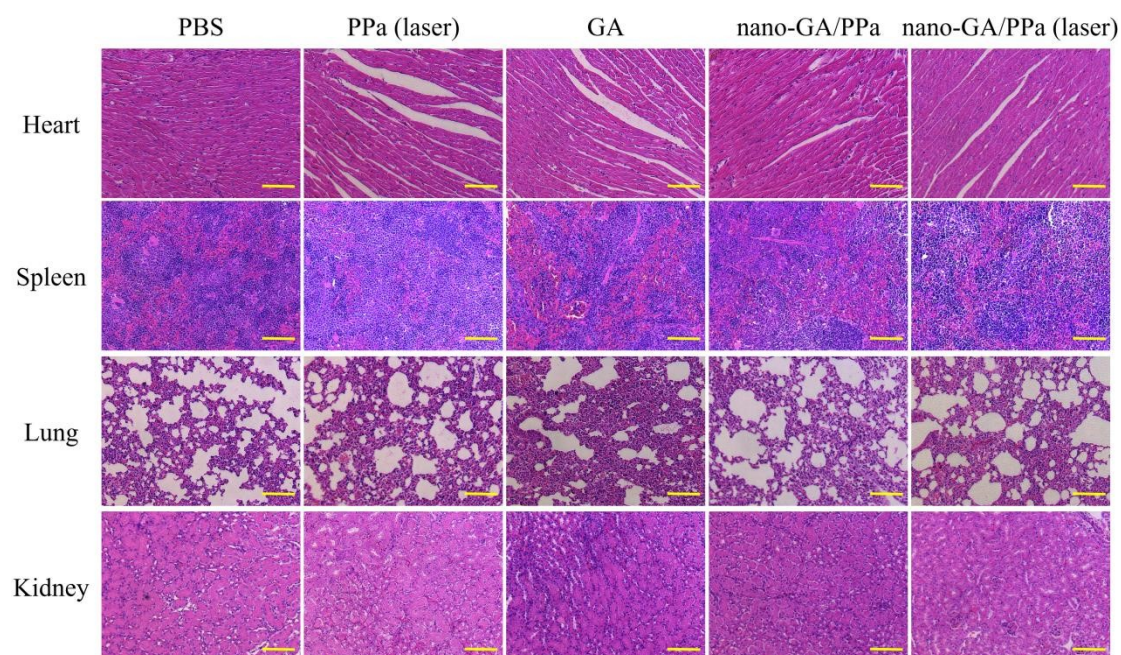


Figure S8. H&E staining of major organs (heart, spleen, lung, and kidney) obtained after various treatments as indicated for 14 days. Scale bar: 50 μm .

Table S1. The UV absorption wavelength at Qy band of nano-GA/PPa prepared at different initial molar ratios of GA to PPa, respectively.

Formulations	PPa	1:6	1:4	1:2	1:1	2:1	4:1	6:1	8:1
Qy (nm)	664	674	670	668	668	669	669	669	670
$Abs_{(Qy\text{-Baseline})}$	---	0.012	0.036	0.069	0.040	0.083	0.065	0.054	0.043

Table S2. Pharmacokinetic parameters of nano-GA/PPa after intravenous administration of equivalent PPa (3.5 mg/kg) in rats (n=3).

Parameters	AUC(0- ∞) ($\mu\text{g}/\text{mL}\cdot\text{h}$)	AUC(0-t) ($\mu\text{g}/\text{mL}\cdot\text{h}$)	CL (L/h/ kg)	MRT(0- ∞) ($\mu\text{g}/\text{mL}\cdot\text{h}$)	T(1/2) (h)	C _{max} ($\mu\text{g}/\text{mL}$)
PPa	12.01 \pm 1.6	9.82 \pm 0.9	1.506	2.24 \pm 0.2	1.69 \pm 0.2	8.25 \pm 1.2
nano-GA/PPa	82.21 \pm 5.3	63.42 \pm 4.6	0.236	7.89 \pm 0.6	6.19 \pm 0.6	19.25 \pm 1. 3

References

1. K. Liu, Y. Kang, G. Ma, H. Mo'hwald and X. Yan, *Phys. Chem. Chem. Phys.*, 2016, 18, 16738–16747.
2. Gaussian 09, Revision E.01, M. J. Frisch, G. W. Trucks, H. B. Schlegel, G. E. Scuseria, M. A. Robb, J. R. Cheeseman, G. Scalmani, V. Barone, B. Mennucci, G. A. Petersson, H. Nakatsuji, M. Caricato, X. Li, H. P. Hratchian, A. F. Izmaylov, J. Bloino, G. Zheng, J. L. Sonnenberg, M. Hada, M. Ehara, K. Toyota, R. Fukuda, J. Hasegawa, M. Ishida, T. Nakajima, Y. Honda, O. Kitao, H. Nakai, T. Vreven, J. A. Montgomery, Jr., J. E. Peralta, F. Ogliaro, M. Bearpark, J. J. Heyd, E. Brothers, K. N. Kudin, V. N. Staroverov, T. Keith, R. Kobayashi, J. Normand, K. Raghavachari, A. Rendell, J. C. Burant, S. S. Iyengar, J. Tomasi, M. Cossi, N. Rega, J. M. Millam, M. Klene, J. E. Knox, J. B. Cross, V. Bakken, C. Adamo, J. Jaramillo, R. Gomperts, R. E. Stratmann, O. Yazyev, A. J. Austin, R. Cammi, C. Pomelli, J. W. Ochterski, R. L. Martin, K. Morokuma, V. G. Zakrzewski, G. A. Voth, P. Salvador, J. J. Dannenberg, S. Dapprich, A. D. Daniels, O. Farkas, J. B. Foresman, J. V. Ortiz, J. Cioslowski, and D. J. Fox, Gaussian, Inc., Wallingford CT, 2013.